Accelerated Publications

Structural Reorganization of the Transferrin C-Lobe and Transferrin Receptor upon Complex Formation: The C-Lobe Binds to the Receptor Helical Domain†

Rutao Liu,[‡,§] Jing-Qu Guan,[‡,§] Olga Zak,[§] Philip Aisen,[§] and Mark R. Chance*[,‡,§,||]

Center for Synchrotron Biosciences, Department of Physiology and Biophysics, and Department of Biochemistry, Albert Einstein College of Medicine, 1300 Morris Park Avenue, Bronx, New York 10461

Received July 23, 2003; Revised Manuscript Received September 15, 2003

ABSTRACT: Human transferrin, a bilobal protein, with each lobe bearing a single iron-binding site, functions to transport iron into cells. While the N-terminal lobe alone does not measurably bind cellular transferrin receptors or serve as an iron donor for cells, the C-lobe is capable of both functions. We used hydroxyl radical-mediated protein footprinting and mass spectrometry to reveal the conformational changes that occur upon complex formation for the human transferrin C-lobe (residues 334−679) bound to the ectodomain of human transferrin receptor 1 (residues 121−760). Oxidation rates for proteolytic peptides in the C-lobe, the receptor, and their complex have been measured by mass spectrometry; upon formation of the complex, a dramatic decrease in modification rates, indicating protection of specific side chain groups, can be seen in C-lobe sequences corresponding to residues 381−401, 415−433, and 457−470. Peptide sequences experiencing modification rate decreases in the transferrin receptor upon C-lobe binding include residues 232−240, 365−371, 496−508, 580 and 581, 614−623, 634−646, 647−681, and 733−760. In addition, several peptides in the receptor exhibit enhancements in the rate of modification consistent with allosteric effects of complex formation. Using tandem mass spectrometry, the sites of modification with altered reactivity in the complex include Met382, Met389, Trp460, Met464, and Phe427 in the C-lobe and Tyr503, Pro581, Tyr611, Leu619, Met635, Phe650, Trp740, Trp754, and Phe760 within the transferrin receptor. Using available genetic, biochemical, and structural data, we confirm that the conserved RGD sequence (residues 646−648) in the helical domain of the transferrin receptor, including residues from Leu619 to Phe650, is a primary binding site for the transferrin C-lobe.

Transferrin (Tf)[1] and the transferrin receptor (TfR) function interactively to provide iron for cells dependent on this essential element (*1*−*3*). Human transferrin is a single-chain, bilobal, iron-binding glycoprotein consisting of 679 amino acids. Each lobe of transferrin is further divided into two dissimilar domains with their iron-binding sites located within the interdomain cleft. Four residues (Asp392, Tyr426, Tyr517, and His585) in the C-lobe serve as iron-binding ligands, complemented by a bidentate carbonate anion linked to protein by a network of hydrogen bonds (*4*). Human TfR 1 is a disulfide-linked homodimer of 90 kDa glycoprotein subunits, each of which is capable of binding two transferrin molecules (*5*−*7*). A second transferrin receptor has recently been described, but its role in iron metabolism is not yet clear (*8*). The major mechanism for uptake of iron by vertebrate cells involves the binding of iron bearing Tf to TfR followed by endocytosis and iron release in the acidic environment of the endosome. The transferrin−receptor complex is then recycled to the cell membrane and free transferrin released. Although crystallographic data for transferrin and its receptor have been available for some time, the structure of the complex has to date not been determined (*4*, *7*).

For the studies presented here, we have chosen to examine the soluble ectodomain of transferrin receptor 1, available as a recombinant protein expressed in a baculovirus system, in a complex with the C-lobe of transferrin, rather than the full-length protein to simplify the analysis of the data. More than 75% of the binding energy of the Tf−TfR complex is due to the C-lobe (*9*), and the absence of glycosylation does

† This research is supported in part by The Biomedical Technology Centers Program of the National Institute for Biomedical Imaging and Bioengineering (Grant P41-EB-01979) and the Innovative Molecular Analysis Technologies Program of the National Cancer Institute (Grant R33-CA-83179) and Grant R01-DK-15056.

* To whom correspondence should be addressed. Phone: (718) 430-4136. Fax: (718) 430-8587. E-mail: mrc@aecom.yu.edu.

‡ Center for Synchrotron Biosciences.

§ Department of Physiology and Biophysics.

|| Department of Biochemistry.

[1] Abbreviations: dTT, dithiothreitol; ESI, electrospray ionization; HFE, hereditary hemochromatosis protein; HPLC, high-pressure liquid chromatography; MS, mass spectrometry; PDB, Protein Data Bank; Tf, transferrin; TfR, transferrin receptor.

10.1021/bi0352973 CCC: $25.00
Published on Web 10/09/2003

not affect the functional properties of transferrin (*10*). Studies of chimeric human/chicken transferrin receptors have indicated that the C-terminal "helical" domain of the receptor (residues 607−760), which provides important contacts within the homodimer interface, is essential for binding to transferrin (*11*). Supporting this idea is a mutagenesis study showing that an RGD sequence (residues 646−648) in the C-terminal region of TfR is crucial for transferrin binding; this RGD recognition motif is functionally important for the binding of many proteins to cells (*12*). The hereditary hemochromatosis protein HFE also binds TfR, and the major site of interaction is with the TfR C-terminal helical domain (*13*). Biochemical evidence that HFE has receptor-binding sites overlapping with those of transferrin (*13*) further implicates this binding site as being critical for the interaction.

Hydroxyl radicals, including those generated through the radiolysis of water by synchrotron radiation, can efficiently oxidize aromatic and sulfur-containing amino acids on the surface of proteins in direct relation to their reactivity and their solvent accessibility (*14*−*18*). In particular, the solvent accessible side chains of cysteine, methionine, phenylalanine, tyrosine, tryptophan, histidine, proline, and leucine provide probes for synchrotron footprinting experiments (*17*−*20*). These residues cover ∼30% of the sequence of a typical protein (*21*; http://prowl.rockefeller.edu/); thus, the method can probe a large number of side chains throughout the protein sequence. Radiolysis of protein samples modifies the reactive and accessible side chain groups; the samples are digested with proteases, separated by reverse-phase liquid chromatography, and analyzed by electrospray ionization mass spectrometry. Modified and unmodified peptides are individually quantitated for a specific exposure time, and the rate of oxidation of peptides containing the susceptible sites is determined by measurements at varying exposure times (*14*, *17*, *18*, *20*, *22*). Footprinting provides only "local" information about the environment of the probe sites. Allosteric changes in conformation induced by ligand binding can give rise to either protections (decreases in side chain reactivity) or enhancements (increases in reactivity) depending on the induced conformational changes (*17*, *18*, *20*, *22*). In the case of protein−protein (*17*, *23*) or protein−DNA (*24*) interactions, formation of a binding interface can give rise to protections. However, confirmation of the interface requires additional biochemical, structural, or genetic data.

Since the crystal structures of both Tf (*4*) and TfR (*7*) have been reported, the accessible and potentially reactive residues of each partner in isolated form can be predicted (see below). Our results showed that the reactivities of peptides composed of sequences of residues 381−401, 415−433, and 457−470 in the transferrin C-lobe are reduced in the complex compared to their reactivities in the isolated forms. Two of these peptides contain ligands for the iron atom, indicating a potential conformational link between the binding event and the structure near the iron site. In the receptor, peptides containing residues 232−240 and 365−371 within the apical domain, residues 496−508, 580, and 581 in the protease domain, and residues 601−613, 614−623, 634−646, 647−681, and 733−760, all in the helical domain (*7*), include side chains that exhibit reduced reactivity upon formation of the complex. Other peptides within the C-lobe and TfR exhibit no significant changes in modification rate upon complex formation. Tandem MS methods identified specific side chains experiencing reactivity changes upon complex formation. The results are interpreted in terms of a predicted binding interface for the C-lobe−receptor complex that includes the conserved RGD sequence of the C-terminal helical domain of the receptor (*12*, *13*). Presumed allosteric changes in the protease and apical domains of the receptor and in the C-lobe are seen to result from complex formation.

EXPERIMENTAL PROCEDURES

Preparation of the Human Transferrin C-Lobe, the Transferrin Receptor, and Their Complex. The soluble ectodomain of human transferrin receptor 1 (hTfR 1), expressed in a baculovirus system, was provided by P. Snow of the California Institute of Technology (Pasadena, CA). This construct is normally glycosylated. The C-lobe of human Tf was obtained by enzymatic cleavage and size-exclusion chromatography as previously described (*9*, *25*). The C-lobe−transferrin receptor complex was prepared by incubating a 2-fold molar excess of the iron-loaded C-lobe with TfR 1 and separating the complex of the two proteins from the uncomplexed components by size-exclusion chromatography (*9*, *25*, *26*). The complex is well-resolved and can be cleanly isolated from the uncomplexed proteins. A chromatogram of the C-lobe−TfR complex purified as described previously (*9*) shows a ratio of A_{465} (due to iron) to A_{280} (due to protein) of 0.013 (*27*). The calculated ratio, using the protein parameter tool of the EXPASY website and previous studies of the C-lobe (*27*), is 0.014, assuming a 1:1 stoichiometry of the C-lobe and receptor monomer. These data confirm that the preparation contains two molecules of the C-lobe bound per TfR homodimer, a critical point in the interpretation of the footprinting results (see Discussion).

Calculation of the Side Chain Solvent Accessibility (SASA). The VADAR 1.2 computer program (PENCE, University of Alberta, Edmonton, AB) was used to calculate the solvent accessible surface areas of all side chains (square angstroms) from the human transferrin C-lobe (PDB file provided by H. Zuccola). The Tf C-lobe structure of the human form is very similar to the high-resolution structure of rabbit serum transferrin (*28*), which also binds to human TfR and is competent in delivering iron to human cells (*29*). For surface area calculations for the transferrin receptor, PDB entry 1CX8 was used, while for the transferrin receptor bound to the hereditary hemochromatosis protein, PDB entry 1A6Z was used. Results are shown in Tables 1 and 2.

Synchrotron Radiolysis of Protein Solutions and Enzymatic Proteolysis. Prior to radiolysis experiments, the transferrin C-lobe, the transferrin receptor, and their complex were dialyzed at 0−4 °C overnight against 20 mM sodium cacodylate (pH 7.0) (*17*). Synchrotron X-ray experiments were performed at beamline X28C of the National Synchrotron Light Source (NSLS) of the Brookhaven National Laboratory (Upton, NY) as previously described (*17*, *30*, *31*). Radiolyzed samples of 100 pmol of C-lobe, receptor, or complex were reduced and partially denatured in 15% acetonitrile by heating at 95 °C for 20 min in 4 mM dithiothreitol (dTT) and cooling on ice. This treatment reduces the methionine sulfoxide (+16) oxidized product to methionine but will not affect methionine sulfones (+32) (*32*). Thus, peptides containing methionine have less apparent

Table 1: Rate Constants for the Modification of the Human Transferrin C-Lobe[a]

Domain	Sequence	Peptide	Rate Constant (s^{-1})	
			C-lobe	Complex
C1	366-380	I E **C** V S A E T T E D **C** I A K 12 0	0.20±0.02	0.16±0.02
C1	381-401	I **M** N G E A D A **M** S L D G G **F** V **Y** I A G K 28 8 7 8 12	**2.17±0.16**	**0.16±0.03**
C1, C2	415-433	S D N **C** E D T **P** E A G **Y** **F** A V A V V K 6 27 9 25	**2.99±0.19**	**0.46±0.05**
C2	457-470	T A G **W** N I **P** **M** G **L** **L** **Y** N K 39 1 0.3 47 9 52	**1.41±0.15**	**0.33±0.04**
C2	512-522	E G **Y** **Y** G **Y** T G A **F** R 13 2 82 4	0.62±0.04	0.61±0.03
C2	546-552	N **P** D **P** **W** A K 100 107 54	1.66±0.05	1.46±0.09
C1	603-623	Q Q Q **H** **L** **F** G S N V T D **C** S G N **F** **C** **L** **F** R 139 71 2 16 19 14 3 2	3.00±0.19	2.90±0.22
C1	650-657	**Y** **L** G E E **Y** V K 23 0 14	0.93±0.09	0.88±0.08
C1	665-677	**C** S T S S **L** **L** E A **C** T **F** R 8 32 19 3 157	2.54±0.08	2.43±0.1

[a] For each peptide, the potentially modifiable residues are outlined within the peptide sequence in bold type, and the solvent accessibility of the potentially modifiable side chains based on an analysis of the crystal structure of the isolated domain (e.g., the surface area, in units of square angstroms) is shown below the one-letter codes. The rate constants shown in bold are significantly different in the case of Tf or TfR vs their complex (within error).

reactivity than in our previous studies where dTT was not required for denaturation and protease digestion, since the singly oxidized sulfoxide products are typically more abundant while the sulfone oxidation products are significantly less abundant (*14*, *17*, *22*). This does not influence the analysis, since the reactivities of individual components are compared to that of the binary complex under identical reaction conditions. Subsequent proteolysis was carried out with sequencing grade modified trypsin (Promega). The protease was added in two aliquots to the protein samples, yielding a final weight-to-weight ratio of 1:30 for trypsin to protein [in 50 mM Tris (pH 7.8)]. Digestions were performed at 37 °C for 15−18 h.

HPLC−MS and MS/MS. Peptide mixtures were separated by HPLC on a Waters 2690 separations module using a C18 reverse-phase column (Vydac, 1.0 mm × 150 mm). After being desalted for 10 min, the HPLC eluate was directed to a Finigan LCQ quadrupole ion trap mass spectrometer as described previously (*17*). A complete trypsin digestion of the isolated Tf C-lobe generates 43 possible peptide products, 34 of which have MWs of >300. Of these 34, 28 peptides were detected by mass spectrometry analysis (covering ∼80% of the protein sequence), and 11 of the 28 peptides experienced detectable modifications after X-ray beam exposure; the other 17 had modification rates near zero. Dose−response data for nine of the peptides could be reproduced in multiple experiments and are reported in Table 1. For TfR, 71 peptides are generated in a complete trypsin digest, of which 63 are in the detectible mass range and 41 were detected (covering ∼70% of the protein sequence). Of these 41, 29 were observed to be modified; data for 27 peptides were reproducible and are reported in Table 2. The modification sites were identified by tandem MS/MS sequencing. A 1.5 *m*/*z* unit range was used during selection of the parent ion for fragmentation (*17*, *22*).

Calculation of Modification Rates. Peptide products were analyzed by HPLC−ESI-MS, and the total ion current data were quantitated to determine the amounts of modified and unmodified peptides (*17*). The unmodified fraction was

Table 2: Modification Rates of Human Transferrin Receptor[a]

Domain	Sequence	Peptide	Rate constant (s^{-1})	
			Receptor	Complex
Protease –like domain	122-128	**L** **Y** **W** D D **L** K 69 170 47 4	**1.36±0.07**	**1.67±0.08**
Protease –like domain	146-155	**L** **L** N E N S **Y** V **P** R 51 0 25 73	0.43±0.04	0.47±0.04
Protease –like domain	181-183	V **W** R 95	0.74±0.05	0.69±0.04
Apical domain	209-224	LV**Y** **L** V E N **P** G G **Y** V A **Y** SK 153 78 1 4 2	1.41±0.11	1.50±0.04
Apical domain	232-240	**L** V **H** A N **F** G T K 0 0 15	**0.18±0.01**	**0.03±0.01**
Apical domain	262-267	I T **F** A E K 35	**1.16±0.09**	**1.53±0.16**
Apical domain	268-287	V A N A E S **L** N A I G V **L** I **Y** **M** D Q T K 74 1 4 9	1.58±0.16	1.67±0.18
Apical domain	326-339	S S G **L** **P** N I **P** V Q T I S R 4 12 2	0.34±0.05	0.36±0.05
Apical domain	365-371	**M** V T S E S K 18	**2.82±0.56**	**0.33±0.02**
Apical domain	375-382	**L** T V S N V **L** K 0 44	1.28±0.08	1.09±0.04
Protease –like domain	386-394	I **L** N I **F** G V I K 61 0	1.08±0.08	0.91±0.11
Protease –like domain	395-409	G **F** V E **P** D **H** **Y** V V V G A Q R 79 44 12 35	**1.40±0.08**	**1.15±0.11**
Protease –like domain	410-418	D A **W** G **P** G A A K 33 10	0.64±0.07	0.76±0.04
Protease –like domain	429-439	**L** A Q **M** **F** S D **M** V L K 0 4 0 0	3.51±0.19	3.50±0.23
Protease –like domain	440-446	D G **F** Q **P** S R 5 0	1.05±0.19	1.14±0.08
Protease –like domain	447-477	S I I **F** A S **W** S A G D **F** G S V G A T E 0 3 1 **W** **L** E G **Y** **L** S S **L** **H** **L** 24 0 87 59 5 19 106	1.50±0.11	1.59±0.11
Protease-like domain	487-495	A V **L** G T S N **F** K 10 17	**1.73±0.17**	**1.34±0.08**
Protease –like domain	496-508	V S A S **P** **L** **L** **Y** T **L** I E K 17 0 0 39 16	**0.43±0.03**	**0.08±0.02**
Protease –like domain	580-585	I **P** E **L** N K 84 0	**1.73±0.14**	**0.22±0.05**
Protease –like domain	589-600	S S S E V A G Q **F** V I K 1	**0.29±0.03**	**0.41±0.04**
Protease-like domain and helical domain	601-613	**L** T **H** D V E **L** N **L** D **Y** E R 2 37 1 2 16	**0.61±0.04**	**0.37±0.06**
helical domain	614-623	**Y** N S Q **L** **L** S **F** V R 0 0 65 13	**0.69±0.1**	**0.04±0.02**
helical domain	634-646	E **M** G **L** S **L** Q **W** **L** **Y** S A R 10 28 6 135 2 76	**2.13±0.12**	**0.17±0.04**
helical domain	647-651	G D **F** **F** R 1 103	**1.69±0.1**	**0.13±0.03**
helical domain	681-693	V E **Y** **H** **F** **L** S **P** **Y** V S **P** K 38 54 0 1 66 88 23	0.49±0.05	0.42±0.04
Helical domain	699-717	**H** V **F** **W** G S G S **H** T **L** **P** A **L** **L** 0 7 43 18 3 67 1 16 E N **L** K 0	0.56±0.05	0.50±0.06
Helical domain	733-760	N Q **L** A **L** A T **W** T I Q G A A N 18 70 5 A **L** S G D V **W** D I D N E **F** 1 211 84	**0.90±0.06**	**0.11±0.02**

[a] For each peptide, the potentially modifiable residues are outlined within the peptide sequence in bold type, and the solvent accessibility of the potentially modifiable side chains based on an analysis of the crystal structure of the isolated domain (e.g., the surface area, in units of square angstroms) is shown below the one-letter codes.

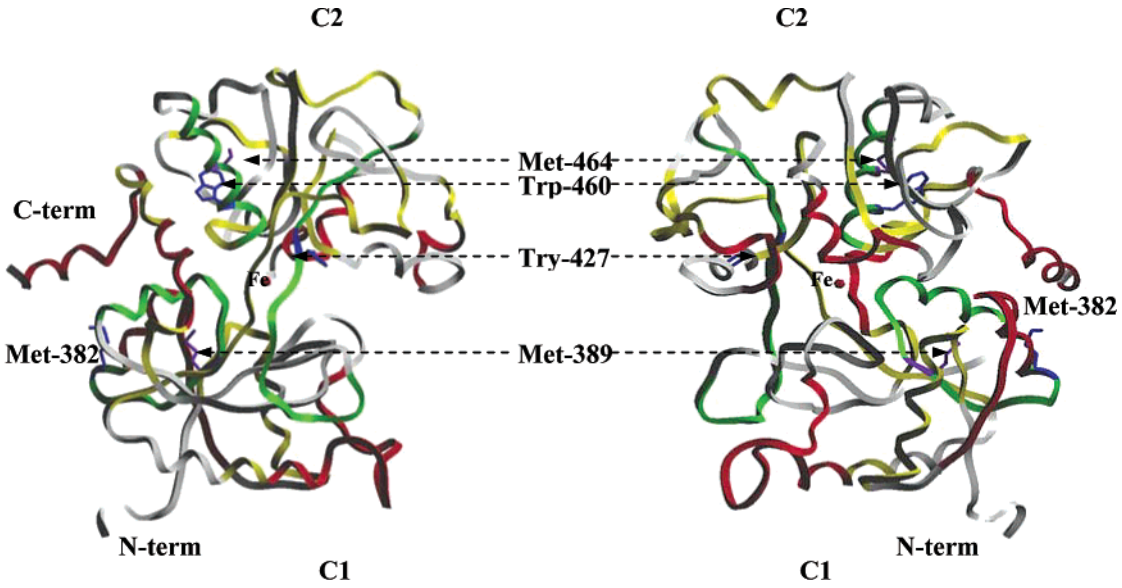

FIGURE 1: Structure of the Tf C-lobe. Two views of the Tf C-lobe related by a 180° rotation about the vertical axis. The modified and protected peptides are shown in green (Met382, Tyr427, and Trp460 side chains in blue and Met389 and Met464 side chains in purple); the modified but not protected peptides are shown in red. The detected but not modified peptides are shown in yellow; the undetected peptides are shown in white. The red ball is the iron atom bound in the C-lobe.

calculated from the ratio of the area under the ion signals for the unoxidized peptides to the total of those for the unoxidized peptides and their radiolytic products. Background modification seen for the methionine-containing peptides in the unexposed sample was subtracted from the total. The unmodified fraction for each peptide at each time point was normalized to that at zero exposure time, where the unmodified fraction is 1.0. The fraction of unmodified peptide was fit to the equation $Y = Y_0e^{-kt}$ using Origin 6.1 (Microcal Software, Inc., Northampton, MA), where Y and Y_0 are the fraction of unmodified peptide at times t and 0 (seconds), respectively, and k is the first-order rate constant. Dose−response curves are presented as the unmodified fraction (plotted on a logarithmic scale) versus X-ray exposure time. Synchrotron exposure times of up to 250 ms result in ~5−60% oxidation of the reactive residues for the individual peptides. Independent experiments on isolated Tf, TfR, and the binary complex were performed three times, and the separate data sets were combined and globally fit using Origin. The reported errors represent the 95% confidence limits as reported by Origin 6.1 using a linear approximation (*17*, *24*).

RESULTS

Reactivity of Transferrin C-Lobe Peptides. Rates of oxidation for nine peptides from the C-lobe and its binary complex with the receptor are shown in Table 1. For each peptide in the table, the potentially modifiable residues are outlined within the peptide sequence in bold type, and the solvent accessibility of the potentially modifiable side chains based on an analysis of the crystal structure of the isolated domain (e.g., the surface area, in units of square angstroms) is shown below the one-letter codes. For example, in Table 1, the rate of modification for peptide 381−401 in the case of the isolated Tf C-lobe is 2.17 s^{-1}. Within this sequence, there are multiple potentially reactive residues. Among these, Met382 and Met389 are the most reactive and the former is quite solvent accessible. Figure 1 of the Supporting Information shows sample dose−response curves for three of the peptides from the Tf C-lobe (panels a−c). The rate for peptide 381−401 is seen in Figure 1c of the Supporting Information (data points and curve fit in black). Upon formation of the Tf C-lobe−TfR complex, the rate of oxidation is reduced considerably for this peptide, to 0.16 s^{-1}, as shown in Table 1 and Figure 1c (red) of the Supporting Information. Of the nine peptides for which we report rates of oxidation in the C-lobe, three exhibit significant protections; for the remaining six, rates of oxidation are unchanged within experimental error. Unchanged oxidation rates for these six peptides suggest (but do not prove) that the susceptible residues likely do not experience conformational changes as a consequence of complex formation. The observation of a subset of peptides experiencing no change in oxidation provides confidence that radiolytic oxidation is not artificially suppressed by the increase in the effective concentration of radical targets in the presence of the complex compared to experiments carried out with C-lobe alone. Also, the footprinting methodology that measures the rate of oxidation of unmodified material, along with the overall first-order behavior of dose−response curves, ensures that the native structure is being probed in the experiment (*14*, *17*, *20*, *22*, *24*, *33*).

The locations of these nine peptides analyzed within the C-lobe are shown in Figure 1 superimposed on two views of the Tf C-lobe structure. A four-color scheme is used to illustrate the results. Peptides that were not detected are shown in white. Those detected but not modified (due to the absence or burial of reactive side chains) are shown in yellow. Peptides that were oxidized, but with oxidation rates unaffected by complex formation, are shown in red, while peptides experiencing protection as a function of complex formation are shown in green. The protected peptides are candidates for receptor binding residues or residues experiencing conformational changes due to binding. Using tandem MS data (not shown), we have identified that Met381, Met389, Trp460, Met464, and Phe427 are the primary probes

in the protected peptides (Figure 1). Two of these probes are close in sequence to Tyr426 and Asp392, which are ligands of the iron atom.

Reactivity of Peptides within the Transferrin Receptor. Table 2 presents data for 27 peptides analyzed for TfR, and Figure 1 of the Supporting Information displays dose−response results for five of those peptides (panels d−h). For example, peptide 647−651 within the helical domain contains a highly accessible Phe at position 650; the rate of oxidation for this peptide in isolated TfR is 1.69 s^{-1}. The dose−response curve for this peptide is shown in Figure 1f (black) of the Supporting Information. Upon formation of the Tf C-lobe−TfR complex, the oxidation rate for this peptide is reduced 10-fold to 0.13 s^{-1} [Figure 1f (red) of the Supporting Information]. Of the 27 peptides from the receptor where oxidation was observed, 12 peptides experience no change in reactivity (within error) and 12 exhibit protections ranging from modest reductions of reactivity in several peptides to 90−95% protection for three peptides within the helical domain, including two that contain the RGD sequence. Three peptides exhibit enhanced reactivity presumably as a result of conformational changes leading to increased surface exposure.

Figure 2 presents the crystallographic structure of TfR (*7*): peptides exhibiting protections shown in green, those exhibiting no changes in red, and those that are observed to be unmodified in yellow. Each TfR monomer contains an apical domain, a protease domain, and a helical domain, the latter providing the bulk of the dimer interface. Protection is observed in three peptides within the apical domain (residues 232−240, 365−371, and 375−382), in four peptides within the protease domain (residues 395−409, 487−495, 496−508, and 580−585), and in four peptides within the helical domain (residues 601−613, 614−623, 634−646, and 647−651). Enhancements in reactivity, likely indicative of allosteric change, are seen in the protease domain and the apical domains. Tandem MS studies (data not shown) demonstrate that Phe760, Trp754, Trp740, Phe650, Met635, Leu619, and Tyr611 are specifically protected within the helical domain, and Pro581 and Tyr503 are specifically protected within the protease domain in the Tf−TfR complex.

DISCUSSION

Transferrin-Mediated Iron Transport. The mechanism of iron uptake from Tf involves binding of iron-bearing Tf to its high-affinity cell surface receptor followed by internalization to endosomes where the lowered pH induces iron release (*1*−*3*, *34*). Many of the conformational changes in Tf that accompany binding and release of iron have been illustrated by crystallography (*4*, *35*−*41*). Transferrin, a bilobal protein with similarly folded N- and C-terminal domains, is further divided into N1 and N2 and C1 and C2 subdomains. Each of the N- and C-lobes binds a single iron atom near the interdomain cleft. The structure of the C-terminal domain, used in this study, is shown in Figure 1. The structure of the transferrin receptor has also been determined (Figure 2), both in the isolated form and bound to the hereditary hemochromatosis protein HFE (*7*, *13*). However, a lack of information about the details of the Tf−TfR interface, and the conformational changes induced upon complex formation, remain important problems to be addressed.

Early investigations indicated that TfR was a homodimer with each monomer binding a molecule of Tf (*5*). Subsequent studies localized the Tf binding site to the C-terminal (helical) domain of each receptor subunit, including a conserved RGD sequence at positions 646−648 (*11*, *12*). Since the HFE protein competes with Tf for binding, its contact interface with TfR also indicates potential points of overlap in the interacting surface of TfR. Specifically, HFE interacts with TfR across portions of two of the helices of the helical domain, a region that spans residues 616−651 of TfR (*13*). In this work, we have used hydroxyl radical-mediated protein footprinting to map the molecular footprint of the iron-loaded C-lobe of transferrin on its receptor (and vice versa). The N-terminal lobe of tranferrin alone will not measurably bind to cellular transferrin receptors nor serve as an iron donor for cells; the C-lobe is capable of both functions, indicating that it is the primary receptor recognition site of transferrin (*42*), providing more than 75% of the binding energy of the Tf−TfR complex (*9*). However, the N-lobe enhances binding of the C-lobe to TfR, so the N-lobe does play a role, by either allosterically enhancing binding of the C-lobe, directly binding to TfR, or both (*43*−*45*).

The Transferrin Receptor Helical Domain Is the Primary Binding Site for the C-Lobe of Transferrin. Three peptides of TfR exhibit reductions in reactivity exceeding 90% (Table 2): TfR peptide 614−623, for which MS/MS identifies Leu619 as the probe residue, TfR peptide 634−646, with Met635 as a probe residue, and TfR peptide 647−651, with Phe650 as a probe residue. These three peptides, which are illustrated in green along with several key probe residues in Figure 2d, include specific residues identified from crystallographic analysis of the HFE−TfR complex as being within the binding interface (*13*); the last two peptides include the essential RGD binding sequence (*12*). The ability of HFE to compete with Tf for receptor binding indicates significant overlap in the interacting regions of the receptor. Bennett et al. (*13*) examined the extent of buried surface area in the HFE−TfR complex, and found that Leu619 and Phe650 contributed 17% of the total interface surface area. We re-examined this interface using the VADAR algorithm and compared the solvent accessible surface area for each residue in the complex and then compared the calculation to one with HFE removed (these latter values were very similar to those of isolated TfR seen in Table 2). This analysis showed that Phe650 in the HFE−TfR complex has an accessible surface area of 11 $Å^2$, compared to an area of 103 $Å^2$ when HFE is removed, while Leu619 has an accessible surface area of 0 $Å^2$ in the complex compared to an area of 65 $Å^2$ when HFE is removed. These accessible surface area reductions are entirely consistent with the >90% decrease in reactivity observed as a function of complex formation for peptide 614−623 (with Leu619 as a probe), peptide 634−646 (with Met635 as a probe), and peptide 647−651 (with Phe650 as a probe) (*17*, *23*, *24*). Not only are the >90% reductions in reactivity seen for these three peptides consistent with the burial of the target residues predicted by analogies between the Tf−TfR and HFE−TfR interactions, they indicate that the protected site of TfR is more than 90% occupied by the C-lobe. Quantitative footprinting measures the ensemble average properties of the population (*33*), and chromatography (see Experimental Procedures) verifies that two molecules of the C-lobe are bound to the TfR homo-

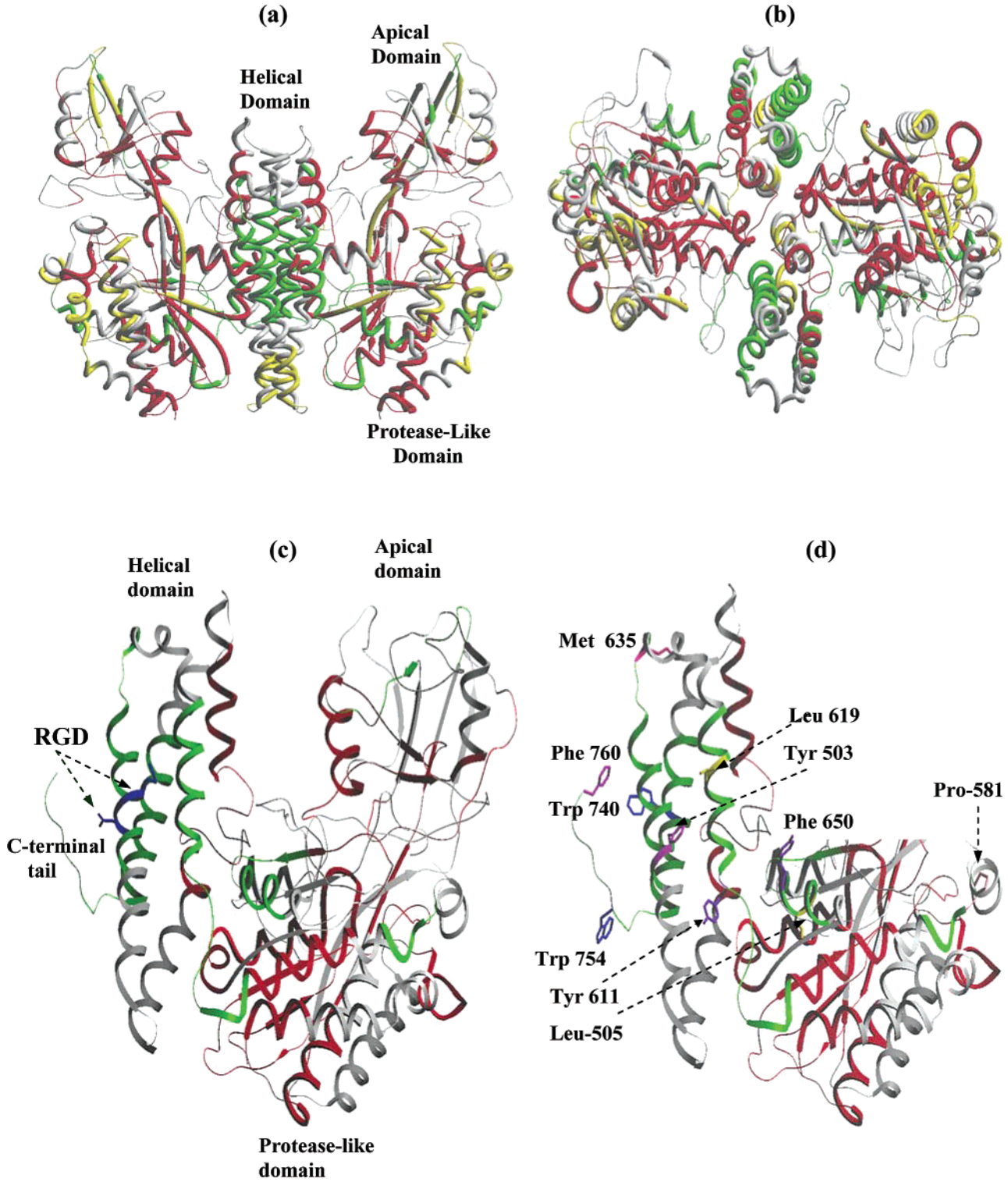

FIGURE 2: Structure of the ectodomain of the Tf receptor dimer (a) and rotation by 90° around the horizontal axis (b). The modified and protected peptides are shown in green; the modified but not protected peptides are shown in red, and the detected and not modified peptides are shown in yellow. The undetected peptides are shown in white. Ectodomain of the TfR monomer with the critical RGD sequence labeled (c) and close-up of the helical part of the protease-like domain with key residues labeled (d).

dimer. Essentially the entire population of C-lobe molecules must be bound only at the indicated sites within the helical domain, or the loss of reactivity would not be so complete. For example, if 50% of the C-lobe molecules were bound to the helical domain and 50% to a different site, the loss of reactivity at the helical domain site could not exceed 50%.

Other evidence that residues identified in the HFE−TfR interface are relevant to Tf−TFR binding includes a TfR mutagenesis study of interfacial residues identified by crystallography, in which selected mutants were specifically examined for Tf binding. Substitutions of five TfR residues at the HFE binding site (Leu619Ala, Arg629Ala, Tyr643Ala, Gly647Ala, and Phe650Gln) resulted in significant reductions in Tf binding affinity (*46*). Thus, probe residues identified by protein footprinting of the transferrin C-lobe (Phe650, Met635, Leu619, and likely Tyr611 as well), along with the

sequences between them, participate in the C-lobe Tf−TfR interface, providing the primary binding site for the isolated C-lobe.

Structural Reorganizations Induced by Complex Formation. Additional protections and enhancements in TfR as a result of complex formation are observed in the protease and apical domains, probably related to allosterically induced conformational changes upon complex formation. Additional protections can be due to direct contact between the C-lobe and sites within the receptor, or they can be the result of allostery. The data above locate the C-lobe close to the HFE binding site upon TfR binding and indicate >90% occupancy at this site. For any additional protections to be inferred as part of the interface requires that they be close enough to the helical domain for a protein the size of the C-lobe to cover both sites.

HFE binding to TfR induces conformational changes in TfR (*13*). For example, upon complex formation, the helical domain rearranges with respect to the apical and protease domains within the monomer units. Other conformational changes involve the dimer interface, which includes contributions from the C-terminal tail (residues 750−760), a loop in the apical domain (residues 312−328), and a loop in the protease-like domain (residues 469−476) (*13*). We can examine the extent to which HFE-induced conformational changes upon complex formation are recapitulated in the case of C-lobe Tf−TfR complex formation.

Peptide 733−760 (having Trp740, Trp754, and Phe760 as probes), which includes the C-terminal tail, experiences a significant protection upon complex formation, indicating that the dimer interface has been perturbed. Alternatively, peptide 447−477 (the exact probe residue is undefined), which includes the protease domain loop, experiences no change in reactivity. Using the solvent accessibility calculations for TfR (Table 2) compared to those for the HFE−TfR complex (minus the contribution of HFE), we can make predictions for the change in residue accessibility within TfR as a function of formation of the HFE−TfR complex. We calculate that Tyr503 and Leu505 in isolated TfR have solvent accessible surface areas of 39 and 16 Å^2, respectively (calculated from ref *7*), but in the TfR−HFE complex, the accessibility of these residues is reduced by 69 and 92%, respectively (calculated from ref *13*). It should be emphasized that these are not sites of HFE binding; e.g., the calculation of the solvent accessibility for these residues with or without the HFE structure shows no change. Interestingly, peptide 496−508 in TfR (with Tyr503 and Leu505 as likely probe residues) experiences an 81% reduction in reactivity upon C-lobe binding, consistent with the above prediction. Alternatively, Pro581 has no similarly predicted conformational change upon HFE binding, although peptide 580−585 experiences an 87% protection upon binding of the C-lobe. Although these protections may be due to direct contact from the C-lobe, this appears to be unlikely because of the distance from the helical domain and the size of the C-lobe. Thus, we suggest these protections are allosterically induced conformational changes of TfR that may be relevant to the binding and transport of transferrin by TfR. Other changes in structure are seen in the apical domain, which is known to be conformationally flexible (*7*), as well as in the protease domain. These regions are potential targets for mutagenesis for exploring receptor function in iron transport.

Conformational Changes in Transferrin Induced by Complex Formation. In transferrin, three peptides are indicated as being protected upon receptor binding, but the indicated side chain probes do not clearly describe a common interface (Figure 1). Thus, a subset of the protections *may* include the interface with TfR, while the remainder represents conformational readjustments of the C-lobe induced by receptor binding. We were able to conclusively identify the probe residues for each of the protected peptides. For example, the probe for peptide 415−433 is identified as Phe427. This result is quite interesting as this side chain is within a set of sequences that connects the C1 and C2 domains of the molecule and the probe site is adjacent to Tyr426, a ligand of the iron atom. Also, the change in conformation localized in peptide 381−401 protects Met382 and Met389, the latter being in the proximity of another iron ligand, Asp392. To provide additional coverage of the C-lobe sequence, we are using additional proteases (*17*, *20*) to supplement information obtained from the tryptic digestion used here. In addition, to identify the effects of N-lobe binding, studies of full-length transferrin are currently underway.

SUPPORTING INFORMATION AVAILABLE

Dose−response curves for the human Tf C-lobe, the Tf receptor, and their complex. This material is available free of charge via the Internet at http://pubs.acs.org.

REFERENCES

1. Richardson, D. R., and Ponka, P. (1997) *Biochim. Biophys. Acta 1331*, 1−40.
2. Trowbridge, I. S., and Omary, M. B. (1981) *Proc. Natl. Acad. Sci. U.S.A. 78*, 3039−3043.
3. Hunt, R. C., and Marshall-Carlson, L. (1986) *J. Biol. Chem. 261*, 3681−3686.
4. Kurokawa, H., Mikami, B., and Hirose, M. (1995) *J. Mol. Biol. 254*, 196−207.
5. Enns, C. A., and Sussman, H. H. (1981) *J. Biol. Chem. 256*, 9820−9823.
6. Aisen, P., Enns, C., and Wessling-Resnick, M. (2001) *Int. J. Biochem. Cell Biol. 33*, 940−959.
7. Lawrence, C. M., Ray, S., Babyonyshev, M., Galluser, R., Borhani, D. W., and Harrison, S. C. (1999) *Science 286*, 779−782.
8. Vogt, T. M., Blackwell, A. D., Giannetti, A. M., Bjorkman, P. J., and Enns, C. A. (2003) *Blood 101*, 2008−2014.
9. Zak, O., and Aisen, P. (2002) *Biochemistry 41*, 1647−1653.
10. Mason, A. B., Miller, M. K., Funk, W. D., Banfield, D. K., Savage, K. J., Oliver, R. W., Green, B. N., MacGillivray, R. T., and Woodworth, R. C. (1993) *Biochemistry 32*, 5472−5479.
11. Buchegger, F., Trowbridge, I. S., Liu, L. F., White, S., and Collawn, J. F. (1996) *Eur. J. Biochem. 235*, 9−17.
12. Dubljevic, V., Sali, A., and Goding, J. W. (1999) *Biochem. J. 341* (Part 1), 11−14.
13. Bennett, M. J., Lebron, J. A., and Bjorkman, P. J. (2000) *Nature 403*, 46−53.
14. Kiselar, J. G., Maleknia, S. D., Sullivan, M., Downard, K. M., and Chance, M. R. (2002) *Int. J. Radiat. Biol. 78*, 101−114.
15. Chance, M. R. (2001) *Biochem. Biophys. Res. Commun. 287*, 614−621.
16. Sharp, J. S., Becker, J. M., and Hettich, R. L. (2003) *Anal. Biochem. 313*, 216−225.
17. Guan, J. Q., Vorobiev, S., Almo, S. C., and Chance, M. R. (2002) *Biochemistry 41*, 5765−5775.
18. Kiselar, J. G., Janmey, P. A., Almo, S., and Chance, M. R. (2003) *Mol. Cell. Proteomics* (in press).
19. Maleknia, S. D., Brenowitz, M., and Chance, M. R. (1999) *Anal. Chem. 71*, 3965−3973.
20. Guan, J. G., Almo, S. C., Reisler, E., and Chance, M. R. (2003) *Biochemistry* (in press).

21. Fenyo, D., Zhang, W., Chait, B. T., and Beavis, R. C. (1996) *Anal. Chem. 68*, 721A−726A.
22. Kiselar, J. G., Janmey, P. A., Almo, S. C., and Chance, M. R. (2003) *Proc. Natl. Acad. Sci. U.S.A. 100*, 3942−3947.
23. Goldsmith, S. C., Guan, J. Q., Almo, S., and Chance, M. (2001) *J. Biomol. Struct. Dyn. 19*, 405−418.
24. Rashidzadeh, H., Khrapunov, S., Chance, M. R., and Brenowitz, M. (2003) *Biochemistry 42*, 3655−3665.
25. Zak, O., and Aisen, P. (2003) *Protein Expression Purif. 28*, 120−124.
26. Egan, T. J., Zak, O., and Aisen, P. (1993) *Biochemistry 32*, 8162−8167.
27. Zak, O., and Aisen, P. (2003) *Biochemistry* (in press).
28. Hall, D. R., Hadden, J. M., Leonard, G. A., Bailey, S., Neu, M., Winn, M., and Lindley, P. F. (2002) *Acta Crystallogr. D58*, 70−80.
29. Lim, B. C., McArdle, H. J., and Morgan, E. H. (1987) *J. Comp. Physiol., B 157*, 363−371.
30. Maleknia, S. D., Ralston, C. Y., Brenowitz, M. D., Downard, K. M., and Chance, M. R. (2001) *Anal. Biochem. 289*, 103−115.
31. Ralston, C. Y., Sclavi, B., Sullivan, M., Deras, M. L., Woodson, S. A., Chance, M. R., and Brenowitz, M. (2000) *Methods Enzymol. 317*, 353−368.
32. Vogt, W. (1995) *Free Radical Biol. Med. 18*, 93−105.
33. Guan, J. Q., and Chance, M. R. (2003) *Encyclopedia of Molecular Cell Biology and Molecular Medicine* (Meyers, R., Ed.) 2nd ed., Wiley, New York.
34. Klausner, R. D., Ashwell, G., van Renswoude, J., Harford, J. B., and Bridges, K. R. (1983) *Proc. Natl. Acad. Sci. U.S.A. 80*, 2263−2266.
35. Karthikeyan, S., Yadav, S., Paramasivam, M., Srinivasan, A., and Singh, T. P. (2000) *Acta Crystallogr. D56* (Part 6), 684−689.
36. Kurokawa, H., Dewan, J. C., Mikami, B., Sacchettini, J. C., and Hirose, M. (1999) *J. Biol. Chem. 274*, 28445−28452.
37. Anderson, B. F., Baker, H. M., Dodson, E. J., Norris, G. E., Rumball, S. V., Waters, J. M., and Baker, E. N. (1987) *Proc. Natl. Acad. Sci. U.S.A. 84*, 1769−1773.
38. Anderson, B. F., Baker, H. M., Norris, G. E., Rice, D. W., and Baker, E. N. (1989) *J. Mol. Biol. 209*, 711−734.
39. Anderson, B. F., Baker, H. M., Norris, G. E., Rumball, S. V., and Baker, E. N. (1990) *Nature 344*, 784−787.
40. Bailey, S., Evans, R. W., Garratt, R. C., Gorinsky, B., Hasnain, S., Horsburgh, C., Jhoti, H., Lindley, P. F., Mydin, A., Sarra, R., et al. (1988) *Biochemistry 27*, 5804−5812.
41. Baker, H. M., Mason, A. B., He, Q. Y., MacGillivray, R. T., and Baker, E. N. (2001) *Biochemistry 40*, 11670−11675.
42. Alcantara, J., Yu, R. H., and Schryvers, A. B. (1993) *Mol. Microbiol. 8*, 1135−1143.
43. Zak, O., Ikuta, K., and Aisen, P. (2002) *Biochemistry 41*, 7416−7423.
44. Zak, O., Trinder, D., and Aisen, P. (1994) *J. Biol. Chem. 269*, 7110−7114.
45. Mason, A. B., Tam, B. M., Woodworth, R. C., Oliver, R. W., Green, B. N., Lin, L. N., Brandts, J. F., Savage, K. J., Lineback, J. A., and MacGillivray, R. T. (1997) *Biochem. J. 326* (Part 1), 77−85.
46. West, A. P., Jr., Giannetti, A. M., Herr, A. B., Bennett, M. J., Nangiana, J. S., Pierce, J. R., Weiner, L. P., Snow, P. M., and Bjorkman, P. J. (2001) *J. Mol. Biol. 313*, 385−397.

BI0352973